The Nature of the Monomer Insertion Step in the Allylnickel(II)-Catalyzed 1,4-Polymerization of 1,3-Butadiene: σ-Allyl-Insertion Mechanism versus π-Allyl-Insertion Mechanism

Sven Tobisch*[a]

Abstract: We present a theoretical investigation on the nature of the monomer insertion step in the allylnickel(II)-catalyzed 1,4-polymerization of 1,3-butadiene that employed a gradient-corrected DFT method. We have explored critical elementary steps of the whole polymerization cycle for the *trans*-1,4 regulating cationic allylnickel(II) $[RC_3H_4Ni^{II}(C_4H_6)L]^+$ catalyst. These steps are i) *cis*-butadiene insertion into either the η^1-σ-butenyl–Ni^{II} bond (σ-allyl insertion mechanism) or the η^3-π-butenyl–Ni^{II} bond (π-allyl insertion mechanism) along with competing pathways for generation of *trans*-1,4 and *cis*-1,4 polymer units, and ii) *anti*–*syn* isomerization. Based on the analysis of geometric and electronic structures of key species involved and the energetics, we present a detailed insight into the different nature of the monomer insertion step according to the two mechanistic alternatives. An understanding of why the π-allyl insertion mechanism is favored over the σ-allyl insertion mechanism is provided. η^1-σ-butenyl–Ni^{II} Species are predicted to be sparsely populated and also distinctly less reactive than η^3-π-butenyl–Ni^{II} species. Although they are commonly believed to be reactive intermediates, η^1-σ-butenyl–Ni^{II} species are, therefore, not likely to be involved along viable pathways for *cis*-butadiene insertion into the butenyl–Ni^{II} bond. The present investigation corroborates our previous conclusion that the π-allyl insertion mechanism represents the preferred mechanism for the monomer insertion step in the allylnickel(II)-catalyzed 1,4-polymerization of 1,3-butadiene. On the other hand, the suggested alternative σ-allyl insertion mechanism has to be considered to be not operative, for both thermodynamic and kinetic reasons. Furthermore, the σ-allyl insertion mechanism would neither provide a rationalization of *cis*–*trans* selectivity nor of chemoselectivity in the allylnickel(II)-catalyzed 1,4-polymerization of 1,3-butadiene.

Keywords: allylic compounds · density functional calculations · nickel · reaction mechanisms · polymerization

Introduction

The polymerization of 1,3-dienes catalyzed by transition metal complexes is a key process in the worldwide chemistry industry.[1]

From a mechanistic point of view, diene polymerization represents one of the most fascinating and challenging subjects in the field of the transition metal-assisted C–C coupling reactions.[2] The transition metal-catalyzed polymerization of butadiene is characterized by i) a high regioselectivity (i.e., it yields a polybutadiene that almost exclusively consists of one type of monomer, namely 1,4 or 1,2), and ii) a high degree of stereoselectivity reached in the C–C coupling reaction.[3] Four highly stereoregular polybutadienes were obtained with different catalysts, namely *cis*-1,4- and *trans*-1,4-polybutadiene and the stereoregular isotactic and syndiotactic forms of 1,2-polybutadiene.

Among the various transition metal-based catalysts for stereospecific polymerization of 1,3-butadiene, the allylnickel(II) complexes, in particular, represent catalysts that were mechanistically studied in the most detailed fashion by experiment.[4–6] In a series of investigations we have theoretically explored the entire catalytic cycles for all established types of structurally defined allylnickel(II) catalysts. The catalysts are: the *trans*-1,4 regulating cationic butenyl(monoligand)(butadiene)nickel(II) $[(\eta^3\text{-}RC_3H_4)Ni^{II}(C_4H_6)L]^+$ complexes ($L = PR_3$, $P(OR)_3$),[7b] the *cis*-1,4 regulating cationic polybutadienyl(butadiene)nickel(II) $[(\eta^3,\eta^2\text{-}RC_7H_{10})Ni^{II}(C_4H_6)]^+$ complexes[7c] and the neutral dimeric allylnickel(II) halides $[(\eta^3\text{-}RC_3H_4)Ni^{II}X]_2$, which either catalyze the formation of a 1,4-polybutadiene consisting predominantly of a *cis*-1,4 structure ($X^- = Cl^-$), or of a *trans*-1,4 structure ($X^- = I^-$), or of a

[a] Dr. S. Tobisch
Institut für Anorganische Chemie
der Martin-Luther-Universität Halle-Wittenberg
Fachbereich Chemie, 06120 Halle (Germany)
Fax: (+49) 345-5527028
E-mail: tobisch@chemie.uni-halle.de

Supporting information for this article is available on the WWW under http://www.chemeurj.org/ or from the author.

0947-6539/02/0820-4756 $ 20.00+.50/0 *Chem. Eur. J.* **2002**, *8*, No. 20

statistical equibinary 1,4-polybutadiene ($X^- = Br^-$).[7d] Based on these investigations we have recently presented a theoretically well-founded, comprehensive view of the *cis–trans* regulation for the allylnickel(II)-catalyzed 1,4-polymerization of butadiene.[8]

Transition metal catalyzed butadiene polymerization is an insertion polymerization.[9] Chain growth proceeds in consecutive steps, starting with the coordination of the monomer followed by the intramolecular migratory insertion into the allyl–transition metal bond. The η^3-π and η^1-σ coordination modes, in general, can represent the reactive form of the allyl–transition metal bond, as illustrated in Figure 1. Cossee

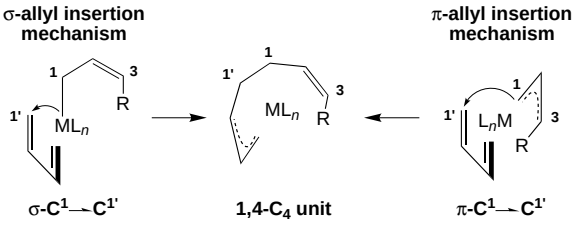

Figure 1. Metal-mediated C–C bond formation between butadiene and the allylic group achieved as a C^1–C^1 linkage according to the σ-allyl- and π-allyl insertion mechanism.

and Arlman suggested that the butenyl group reacts from the η^1-σ mode.[10] Indeed, butadiene insertion into the Ni^{II}–L σ-bond has been established for the Ni–methyl and Ni–aryl bonds,[11a] as well as for the Ni–hydrido bond.[11b] Until recently, the σ-allyl insertion mechanism[10] was believed to be the preferred mechanistic alternative for the monomer insertion step in the 1,3-diene polymerization.[12]

According to the generally accepted *anti–cis* and *syn–trans* correlation,[2b] the configuration of the terminal η^3-butenyl group in the kinetic insertion product is determined by the configuration of the inserting monomer. An *anti*- or *syn*-η^3-butenyl terminal group is formed by butadiene insertion proceeding from the *s-cis* (*anti* insertion) or *s-trans* (*syn* insertion) configuration, respectively. Additionally, butadiene insertion gives rise to a *cis* or a *trans* double bond in the newly formed polymer unit of the growing polymer chain, when starting from an *anti*- or *syn*-butenyl group. Both aspects of the *anti–cis* and *syn–trans* correlation are schematically depicted in Figure 2.

It has been demonstrated by our theoretical investigations[7] that for allylnickel(II) catalysts, chain propagation is most likely to take place via *cis*-butadiene insertion into the η^3-allyl–Ni^{II} bond, according to the π-allyl insertion mechanism proposed by Taube et al.[13] A similar mechanism was also reported for olefin insertion into the allyl–Zr^{III} bond, where the olefin insertion into the η^3-allyl–Zr bond was theoretically predicted as the kinetically preferred route.[14] Furthermore, preliminary results for the allyltitanium(III)-catalyzed polymerization of butadiene indicate that η^3-allyl–Ti^{III} species are involved along the most feasible pathway for monomer insertion.[15] This would suggest that for 1,3-diene insertion as well as for olefin insertion into the allyl–transition metal bond, the η^3-π mode is likely to be considered as the reactive form.[16]

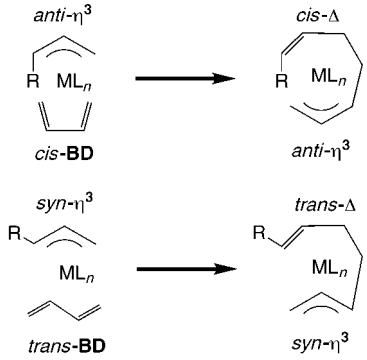

Figure 2. *anti–cis* and *syn–trans* Correlation of the metal-assisted 1,4-polymerization of 1,3-butadiene (R denotes the growing polybutadienyl chain).

The present theoretical investigation is aimed at enhancing the mechanistic insight into the transition metal-catalyzed polymerization of 1,3-dienes further by examining in detail the σ-allyl mechanism for the monomer insertion step. The investigation was carried out for the experimentally well-characterized allylnickel(II) complex $[(\eta^3\text{-}C_3H_5)Ni^{II}(P(OPh)_3)_2]PF_6$,[6e] that catalyzes the formation of a *trans*-1,4-polybutadiene almost exclusively. The thermodynamic and kinetic aspects of the entire catalytic cycle for this type of catalyst have already been presented in our previous study,[7b] where we had focused exclusively on the π-allyl insertion mechanism. Based on our previous results, the present investigation allows us to elucidate the similarities and differences between the two proposed mechanistic alternatives for the monomer insertion step by comparison of the involved key structures. This will provide a detailed understanding as to why the π-allyl insertion mechanism is the operative mechanistic alternative and which crucial factors impede monomer insertion according to the σ-allyl mechanism. The final section is devoted to the implications that the σ-allyl insertion mechanism would have on the stereoregulation of the polymerization process.

Catalytic reaction cycle: Based on the original proposal of Taube et al.,[6e, 13b, 13c] Scheme 1 displays the catalytic cycle for the butenyl(monoligand)(butadiene)nickel(II) catalyst that contains alternative reaction routes for monomer insertion according to the two mechanistic proposals, namely the σ-allyl insertion mechanism along $k_1(\sigma)$ and the π-allyl insertion mechanism along $k_1(\pi)$, respectively. Starting from the $[(\eta^3\text{-butenyl})Ni^{II}L_2]^+$ precatalyst **1**, which predominantly exists in the thermodynamically more stable *syn* form **1s** (ratio of *anti* (**1a**):*syn* (**1s**) ≈ 1:9),[6e] the reaction channel that generates a *trans*-1,4-polybutadiene is accessible along K_1 by substitution of the ligand L by butadiene. This leads to the formation of the butadiene π-complex $[RC_3H_4Ni^{II}(C_4H_6)L]^+$ (**2**), which is the catalytically active species. η^3-π- and $\eta^1(C^1)$-σ-Butenyl forms of **2**, namely **2π** and **2σ**, represent the direct precursors for *cis*-butadiene insertion into either the η^3-butenyl–Ni^{II} bond along $k_1(\pi)$ or into the $\eta^1(C^1)$-butenyl–Ni^{II} bond along $k_1(\sigma)$, which takes places through the transition states **3σ** and **3π**, respectively. *trans*-1,4 and *cis*-1,4 Polymer units are formed by *cis*-butadiene insertion into the *syn*- and *anti*-butenyl–Ni^{II} bond

  0947-6539/02/0820-4757 $ 20.00+.50/0

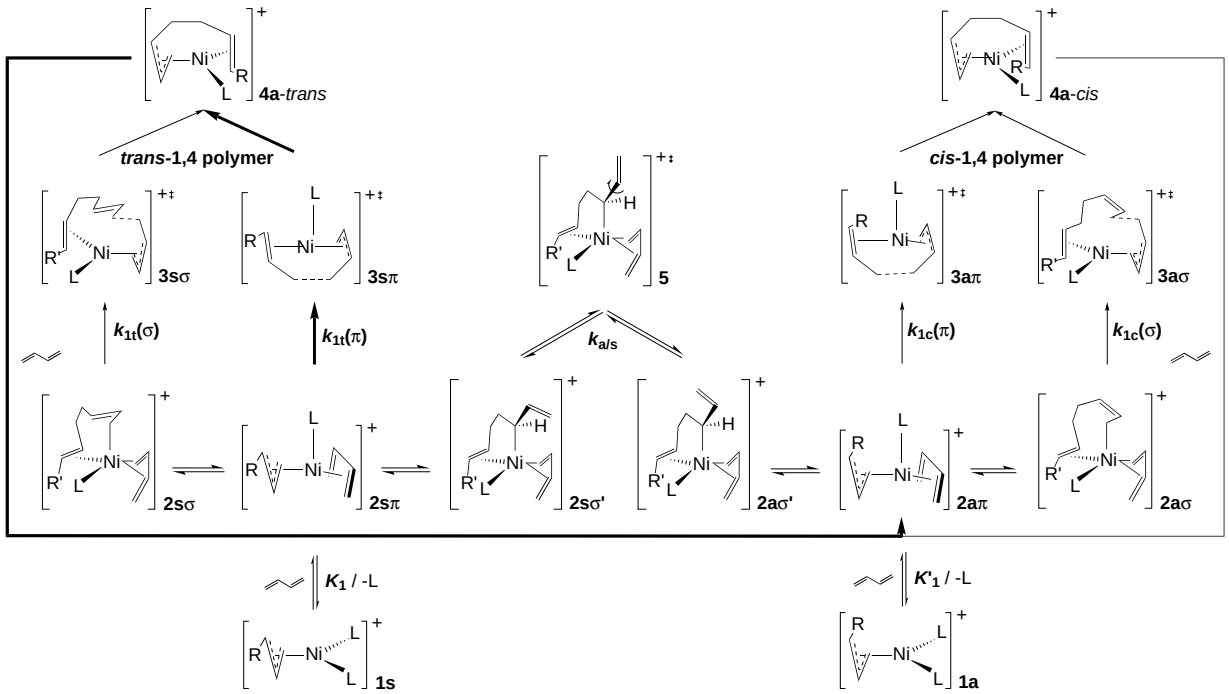

Scheme 1. Catalytic cycle of the 1,4-polymerization of 1,3-butadiene with the cationic butenyl(monoligand)(butadiene)nickel(II) $[(RC_3H_4)Ni^{II}(cis\text{-}C_4H_6)L]^+$ complex as the active catalyst complex. *cis*-Butadiene insertion into the $\eta^1(C^1)$-σ-butenyl–Ni^{II} bond along the $k_1(\sigma)$ route and into the η^3-π-butenyl–Ni^{II} bond along $k_1(\pi)$ is included. The conformations of the key species (for notation see the text) involved along different reaction paths are schematically depicted.

along the competing k_{1t} and k_{1c} pathways, respectively. This always affords the *anti*-η^3-butenyl insertion product **4a** under kinetic control. The chain-growth cycle reiterates with formation of **2a** from **4a** by monomer uptake followed by subsequent *anti–syn* isomerization (via **5**) and/or monomer insertion. *anti–syn* Isomerization (along $k_{a/s}$) represents a necessary step in the 1,4-*trans* production cycle (on account of the kinetically preferred *cis*-butadiene insertion). The $\eta^1(C^3)$-σ-butenyl species **2σ′** is the direct precursor of the transition state **5** for *anti–syn* isomerization. The formation of the butadiene π-complex **2** is verified by the dependence of the overall polymerization rate on nickel and butadiene concentrations according to the rate law[13b] $r_p = k_p[Ni][C_4H_6]_0[L]^{-1}$.[17] The equilibrium between different forms of **2**, namely the π-butenyl forms **2π**, and the σ-butenyl forms with either a $\eta^1(C^1)$, **2σ**, or a $\eta^1(C^3)$, **2σ′**, terminal group, and all the substitution equilibria involving butadiene can be reasonably envisioned to occur rapidly and proceed without any significant kinetic barrier. This is in accordance with the common experience in Ni^{II} coordination chemistry, with Ni^{II} in a spin-paired d^8 configuration.[18]

The coordination number of 5 for nickel in different forms of the active catalyst complex **2** was shown in our previous investigations to be a prerequisite for a facile monomer insertion as well as *anti–syn* isomerization.[7, 19] Therefore, it is likely that *cis*-butadiene insertion into the $\eta^1(C^1)$-butenyl–Ni^{II} bond along $k_1(\sigma)$ (i.e., **2σ** → **3σ** → **4a**) as well as *anti–syn* isomerization along $k_{a/s}$ via the $\eta^1(C^3)$-butenyl–Ni^{II} species (**2aσ′** → **5** → **2sσ′**) have to be assisted by coordination of a double bond from the growing polymer chain on Ni. In contrast, the polymer chain is not required to participate in monomer insertion into the η^3-butenyl–Ni^{II} bond along $k_1(\pi)$ (i.e., **2π** → **3π** → **4a**).

Computational Models and Methods

Models: We modeled the real catalyst, the butenyl(monoligand)(butadiene)nickel(II) complex $[RC_3H_4Ni^{II}(C_4H_6)L]^+$ (**2**) by the cationic $[RC_3H_4Ni^{II}(C_4H_6)PH_3]^+$ complex, where PH_3 served as a computationally less demanding model of the real $P(OR)_3$ ligand L. Two model systems were adopted in the present study to represent the coordinating polybutadienyl chain. In the first place we investigated the catalytic cycle with the $\{[(C_4H_7)Ni^{II}(cis\text{-}C_4H_6)PH_3]^+ + C_2H_4\}$ catalyst model **I**, where the butenyl group was mimicked by crotyl (i.e., $R = CH_3$), together with free ethylene to serve as a simplified model for the coordination of a double bond from the polybutadienyl chain other than the double bond that originates from the ultimate inserted butadiene.[20a] Calculations were also carried out for the $[(C_8H_{13})Ni^{II}(cis\text{-}C_4H_6)PH_3]^+$ catalyst model **II**. In this model, the polybutadienyl chain was represented by two subsequent C_4 units. This was done in order to mimic the formation of a chelate ring by coordination of the first double bond of growing polybutadienyl chain to the nickel atom.[20b]

We restricted our examination of the chain propagation step to the *cis*-butadiene insertion, and did not take into consideration the alternative insertion of butadiene from its *s-trans* configuration. A justification for neglecting this reaction pathway has been given in the case of nickel, on both experimental[6e, 11, 21] and theoretical evidence,[7b] which convincingly establishes *cis*-butadiene insertion into Ni–allyl, Ni–alkyl, and Ni–H bonds. The effect of the solvent or the counterion upon the catalytic cycle was neglected. The mechanistic conclusions drawn in the present study, therefore, are valid for polymerization occurring in non-coordinating solvents with weakly coordinating counterions involved. This is indeed the case for the reaction conditions for the polymerization process under

0947-6539/02/0820-4758 $ 20.00+.50/0 *Chem. Eur. J.* **2002**, *8*, No. 20

investigation.[13b, 22] Furthermore, experiments have shown an essentially unchanged *cis*–*trans* selectivity upon variation of both the solvent and the weakly coordinating counterion.[22]

Method: All reported DFT calculations were performed by means of the program package TURBOMOLE, developed by Häser and Ahlrichs.[23] The calculations were carried out with the LDA with Slater's exchange functional[24a,b] and Vosko–Wilk–Nusair parameterization on the homogeneous electron gas for correlation,[24c] augmented with gradient-corrected functionals for electron exchange according to Becke[24d] and correlation according to Perdew[24e] in a selfconsistent fashion. This gradient-corrected density functional is usually termed BP86 in the literature. In recent benchmark computational studies, it was shown that the BP86 functional gives results that are in excellent agreement with the best wave function-based method available today, for the class of reactions investigated here.[25]

For all atoms a standard all-electron basis set of triple-ζ quality for the valence electrons augmented with polarization functions was employed for the geometry optimization and the saddle-point search. The Wachters 14s/9p/5d set,[26a] supplemented by two diffuse p[26a] and one diffuse d function[26b] contracted to (62111111/5111111/3111), was used for nickel, and standard TZVP basis sets[26c] were used for phosphorous (a 13s/9p/1d set contracted to (73111/6111/1)), for carbon (a 10s/6p/1d set contracted to (7111/411/1)), and for hydrogen (a 5s/1p set contracted to (311/1)). The frequency calculations were performed with standard DZVP basis sets,[26c] which consist of a 15s/9p/5d set contracted to (63321/531/41) for nickel, a 12s/8p/1d set contracted to (6321/521/1) for phosphorous, a 9s/5p/1d set contracted to (621/41/1) for carbon, and a 5s set contracted to (41) for hydrogen. The corresponding auxiliary basis sets were used to fit the charge density.[26c,d] This is the standard computational methodology utilized throughout this paper.

The geometry optimization and the saddle-point search were carried out at the BP86 level of approximation by utilizing analytical/numerical gradients/Hessians according to standard algorithms. No symmetry constraints were imposed in any case. The stationary points were identified exactly by the curvature of the potential-energy surface at these points corresponding to the eigenvalues of the Hessian. The reaction and activation enthalpies and free energies (ΔH, $\Delta H^{\neq}$ and ΔG, $\Delta G^{\neq}$ at 298 K and 1 atm) were calculated for the most stable isomers of each of the key species of the entire catalytic reaction. The enthalpies reported for key structures of model system **I** contain zero-point energy corrections (ZPE) and thermal contributions, whereas Gibbs free energies are given for model system **II**. The electronic structure of key structures was analyzed with the natural bond orbital (NBO) population scheme.[27]

Labeling of the molecules: A number of labeling conventions have been adopted throughout this paper. Thus, species of the model system **I** will be referred to by numerals attached to lower-case letters (e.g. **2a**, **2s**), whereas numerals attached to upper-case letters (e.g. **2A**, **2S**) refer to structures of the model system **II**. The following arabic numerals are chosen for key structures: **1** for the precatalyst, **2** for the *cis*-butadiene π-complex, **3** for the transition state for *cis*-butadiene insertion into the butenyl–Ni^{II} bond, **4** for the η^3-butenyl insertion product, and **5** for the transition state for *anti*-*syn* isomerization. The *anti*- and *syn*-butenyl forms of the complexes will be labeled as **a** or **A** and **s** or **S**, respectively. An additional σ and π will be used for notation of **2** and **3** in order to distinguish between η^1-σ- and η^3-π-butenyl–Ni^{II} species. Thus, for example, **3aσ**, **3aπ** and **3sσ**, **3sπ** represent the transition states for monomer insertion along the 1,4-*cis* (along k_{1c}) and 1,4-*trans* (along k_{1t}) generating cycle, with C–C bond formation occurring through *cis*-butadiene insertion into either the $\eta^1(C^1)$-σ-butenyl–Ni^{II} bond (via $k_1(\sigma)$) or the η^3-π-butenyl–Ni^{II} bond (via $k_1(\pi)$) (cf. Scheme 1).

A number of isomers are possible for each species; they were carefully explored. These species differ with respect to the mutual orientation of the reacting butenyl and butadiene moieties, which originate from the different chiralities that can be attained for both the butadiene–Ni^{II} and the butenyl–Ni^{II} coordination (cf. Figure 3). In addition to the commonly used *Re*/*Si* terminology[28] these enantiomers can also be denoted as supine (*exo*) and prone (*endo*).[29, 30] Furthermore, the conformers that are possible, while keeping the chirality of the butadiene–Ni^{II} and the butenyl–Ni^{II} coordination fixed, were carefully explored for each key structure.

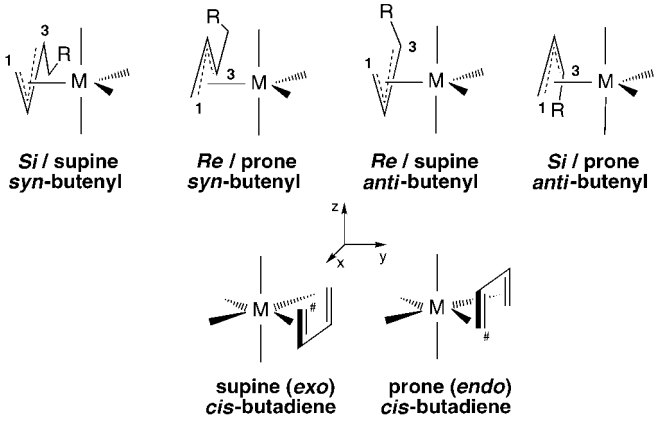

Figure 3. Two enantiomeric forms of the η^3-butenyl–metal (*anti* and *syn* forms) and the η^4-*cis*-butadiene–metal coordination.[30]

Results and Discussion

We shall start our investigation by exploring the $k_1(\sigma)$ route for monomer insertion along competitive pathways and also *anti*–*syn* isomerization[31] by the use of model **I** for the active catalyst complex. The mechanistic insights will be further improved in a subsequent examination of the catalyst model **II**.

Catalyst model I: Among the number of isomeric forms possible for each species (most of which have been carefully explored), only the most stable isomeric forms are reported. For the π-butenyl species **2π** and **3π**, the isomers that arise from the two enantiomeric forms of coordination for each of the two reactive fragments, namely *cis*-butadiene and the η^3-butenyl group in its *anti* and *syn* forms, were explicitly considered. This gives rise to either a supine-supine, supine-prone, prone-supine or prone-prone mutual orientation of the two fragments. Furthermore, with regard to the enantiomers of *cis*-butadiene–Ni^{II} and of *anti*/*syn*-butenyl–Ni^{II} coordination, for the η^1-butenyl species **2σ**, **2σ′**, **3σ**, and **5**, the isomers that originate from the rotation around the σ-butenyl–Ni^{II} bond were examined. Also probed were the isomers that arise from different ligand arrangements around nickel in five-coordinate complexes that adopt either a trigonal-bipyramidal (TBPY) or a square-pyramidal (SPY) structure. We are focusing on activation enthalpies $\Delta H^{\neq}$ and enthalpy differences ΔH, respectively, to examine the differences in reactivity and stability between σ-butenyl and π-butenyl species for catalyst model **I**. This is a consequence of the fact that free ethylene serves as a model for the coordinating polybutadienyl chain.[32] Table 1 summarizes the energetics of key stationary points along the most feasible pathway of different reaction routes. Special emphasis is directed to the stability and reactivity of the two enantiomers of *anti*- and *syn*-butenyl forms. Figure 4 plots the thermochemical profile for competitive pathways for *cis*-butadiene insertion into the η^1-σ- and η^3-π-butenyl–Ni^{II} bond and for *anti*–*syn* isomerization. Also depicted in Figure 4 are the conformations of the species involved along the reaction paths. All optimized structures are provided in the Supporting Information.

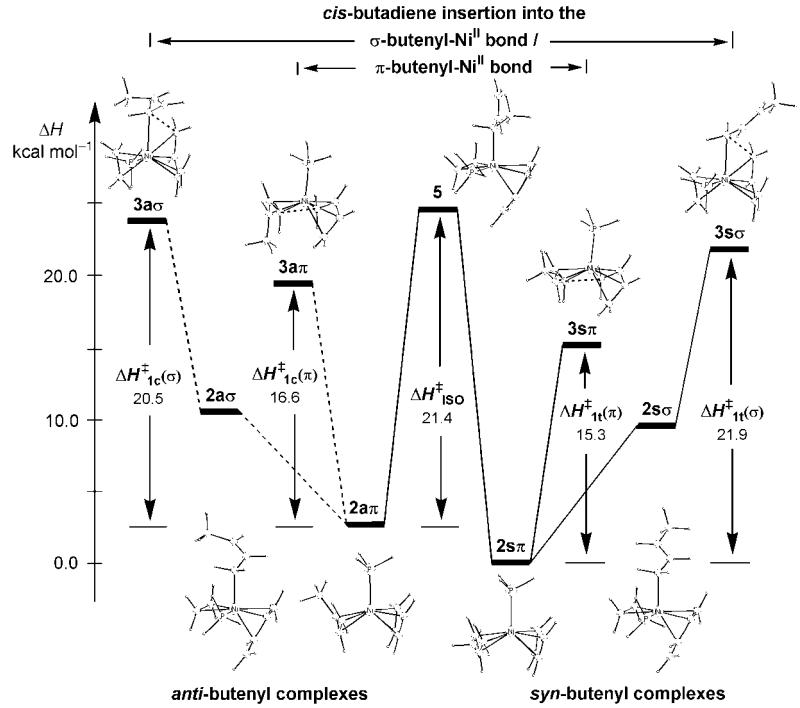

Figure 4. Condensed thermochemical profile (ΔH, $\Delta H^{\ddagger}$ [kcal mol^{-1}]) of competitive pathways to generate *trans*-1,4 (——, along k_{1t}) and *cis*-1,4 (- - - -, along k_{1c}) polymer units for the {[$(C_4H_7)Ni^{II}$(*cis*-C_4H_6)PH_3]$^+$ + C_2H_4} catalyst model **I**, consisting of *cis*-butadiene insertion into the $\eta^1(C^1)$-σ- and the η^3-π-butenyl–Ni^{II} bond and of *anti*–*syn* isomerization.

Table 1. Calculated thermochemical profile (enthalpy) for crucial steps of the polymerization cycle for the {[$(C_4H_7)Ni^{II}$(*cis*-C_4H_6)PH_3]$^+$ + C_2H_4} catalyst model **I**.[a–c]

Category	Description[b]	Species	ΔH, $\Delta H^{\ddagger}$ [kcal mol^{-1}][c]
cis-butadiene π-complex	*syn*-η^3-butenyl (*S*/*P*)	**2sπ**	0.0/2.8
	anti-η^3-butenyl (*S*/*P*)	**2aπ**	2.7/6.6
	syn-$\eta^1(C^1)$-butenyl (*Re*/*Si*)	**2sσ**	9.3/9.6
	anti-$\eta^1(C^1)$-butenyl (*Re*/*Si*)	**2aσ**	10.7/11.0
	syn-$\eta^1(C^3)$-butenyl (*Re*/*Si*)	**2sσ′**	17.0/17.2
	anti-$\eta^1(C^3)$-butenyl (*Re*/*Si*)	**2aσ′**	17.2/17.4
insertion TS	*syn*-η^3-butenyl (*S*/*P*)	**3sπ**	15.5/15.1
	anti-η^3-butenyl (*S*/*P*)	**3aπ**	19.2/19.4
	syn-$\eta^1(C^1)$-butenyl (*Re*/*Si*)	**3sσ**	21.7/22.1
	anti-$\eta^1(C^1)$-butenyl (*Re*/*Si*)	**3aσ**	23.4/23.0
isomerization TS		**5**	24.1

[a] Only the most stable isomer for each species is reported. The two enantiomeric forms for both the *anti*- and *syn*-butenyl–Ni^{II} coordination (cf. Figure 3) are explicitly given for the energetically favored *cis*-butadiene orientation (see text). [b] The enantiomers of the butenyl–Ni^{II} coordination are denoted in the following way. The notation given in parenthesis refers to supine (*S*) or prone (*P*) for η^3-butenyl–Ni^{II} species and to *Re* or *Si* for η^1-butenyl–Ni^{II} species (cf. Figure 3). [c] Enthalpies relative to [(*syn*-η^3-C_4H_7)Ni^{II}(η^4-*cis*-C_4H_6)PH_3]$^+$ **4sπ** + C_2H_4.

Butadiene π-complex: Five-coordinated Ni^{II} compounds with either a square-pyramidal (SPY) or a trigonal-bipyramidal (TBPY) configuration are located as the most stable isomers for π-butenyl (**2π**), and σ-butenyl, (**2σ**, **2σ′**), species, respectively (cf. Figure 4). For both σ-butenyl and π-butenyl species, *cis*-butadiene preferentially coordinates in a bidentate fashion (η^4-*cis*). First, we briefly summarize the results for **2π**, which were already discussed in detail in our previous study,[7b] and follow that up by examining the σ-butenyl forms **2σ** and **2σ′**, respectively.

Species **2π** adopts a SPY configuration with the butenyl group and *cis*-butadiene residing in the square-planar coordination plane while the ligand L occupies the basal position. The thermodynamic stability of different stereoisomers of **2π** is largely determined by the enantioface of *cis*-butadiene involved in coordination, while the influence of the η^3-butenyl group's enantioface upon the stability is less pronounced. The thermodynamically most stable isomers are characterized by a supine *cis*-butadiene coordination (the prone *cis*-butadiene isomers are $\approx$9–11 kcal mol^{-1} higher in energy)[7b] and the difference in stability between the supine and prone π-butenyl forms amounts to $\approx$3–4 kcal mol^{-1} for supine butadiene isomers (ΔH, Table 1). The *syn*-butenyl forms are always thermodynamically more stable than the corresponding *anti*-butenyl isomers. For the most stable supine–supine stereoisomer, the *syn* form is 2.7 kcal mol^{-1} (ΔH, Table 1) more stable than the *anti* form.

For both the $\eta^1(C^1)$-butenyl and the $\eta^1(C^3)$-butenyl η^4-*cis*-butadiene species **2σ** and **2σ′**, respectively, we have TBPY compounds located as the most stable isomers.[33] In **2σ** and **2σ′**, the η^1-butenyl group (which acts as the strongest donor) preferably occupies the axial position, with both the coordinating polybutadienyl chain (mimicked by ethylene) and the ligand L residing on equatorial positions. The η^4-*cis*-butadiene adopts equatorial and axial positions. The axial butadiene coordination *trans* to the η^1-butenyl group, however, is somewhat weakened as a result of competition for coordination with the butenyl group.

The charges on individual atoms and groups for key species of the polymerization cycle collected in Table 2 reveals interesting insights into the electronic nature of the η^3- and η^1-butenyl–Ni^{II} coordination in **2**. The η^3-butenyl–Ni^{II} coordination is seen as an interaction of nickel with a delocalized electron density distribution on the butenyl group. The η^1-butenyl–Ni^{II} coordination, however, is characterized by the accumulation of electron density on either the primary C^1 or the substituted C^3 carbon in **2σ** and **2σ′**, respectively, that interacts with the formally electron-deficient Ni^{II}. Overall, the

  0947-6539/02/0820-4760 $ 20.00+.50/0 *Chem. Eur. J.* **2002**, *8*, No. 20

Table 2. Charges on individual atoms and groups in key stationary points of the polymerization cycle for the $\{[(C_4H_7)Ni^{II}(cis\text{-}C_4H_6)PH_3]^+ + C_2H_4\}$ catalyst model **I**.[a]

Species	C^1H_2	C^2H	C^3H	C^5H_2	Σ_{crotyl}	$\Sigma_{butadiene}$	L/ethylene	Ni
2sπ	0.009	−0.039	0.020	−0.015	0.058	−0.042	0.300/–	0.688
2sσ	−0.082	−0.043	0.098	−0.017	0.040	0.001	0.261/−0.061	0.760
2sσ′	0.105	−0.039	−0.069	−0.027	0.046	0.010	0.245/−0.059	0.758
3sπ	0.058	−0.049	0.015	0.049	0.090	0.000	0.272/–	0.632
3sσ	−0.036	−0.067	0.089	0.006	0.048	−0.016	0.334/−0.086	0.719
5	0.087	−0.077	−0.093	−0.021	−0.042	0.034	0.276/−0.034	0.765

[a] Based on natural population analyses; for atom labels, see Figure 5.

charge distribution indicates a higher polarity of the butenyl–Ni^{II} coordination in the η^1-σ mode ($\eta^1(C^1) > \eta^1(C^3)$) compared to the η^3-π mode.

From the energetics of the most stable isomers of **2π**, **2σ**, and **2σ′** (Table 1) the following conclusions can be drawn with regard to thermodynamic stability of different forms of **2**. i) The π-butenyl species **2π** is the thermodynamically most stable form of **2**. The σ-butenyl species are energetically well-separated from **2π** by 9.5 kcal mol^{-1} (ΔH)[34] for **2σ** and by 17.1 kcal mol^{-1} (ΔH)[34] for **2σ′**. The energetic gap between $\eta^1(C^1)$ and $\eta^1(C^3)$ species amounts to 7.6 kcal mol^{-1} (ΔH),[34] with **2σ** being the favored one. This is attributed to the less effective accumulation of electron density on the substituted C^3 atom compared to that of the primary C^1 atom. Although we have not been able to locate the transition state for the η^3-π → η^1-σ rearrangement of the butenyl group in **2**, the large thermodynamic gap between **2π** and **2σ**, **2σ′** leads us to conclude that the η^1-butenyl species should be sparsely populated under polymerization conditions. ii) For both **2π** and **2σ**, which act as precursors for monomer insertion along $k_1(\pi)$ and $k_1(\sigma)$, respectively, the *syn*-butenyl forms are thermodynamically more stable than the corresponding *anti*-butenyl forms. The difference in stability between *anti* and *syn* forms, however, decreases upon going from η^3-butenyl to η^1-butenyl species. The gap of 2.7 kcal mol^{-1} (ΔH) in favor of **2sπ** is reduced to approximately half for **2σ** where the *syn* form **2sσ** is 1.4 kcal mol^{-1} (ΔH)[34] lower in energy than the *anti* form **2aσ** and ends up with an almost identical stability of *anti* and *syn* forms in **2σ′**. iii) The difference in stability between the two enantiomeric forms of the η^3- and η^1-butenyl–Ni^{II} coordination follows the trend that is very similar to the gap between *anti*- and *syn*-butenyl forms. For **2π**, the supine and prone enantiomers differ by ≈3–4 kcal mol^{-1} (ΔH), whereas the two η^1-butenyl enantiomers become very close in energy for both **2σ** and **2σ′**.

The η^4-*cis*-butadiene π-complex **2** is the catalytically active species, since **2π** and **2σ** represent the direct precursors of the transition states for *cis*-butadiene insertion into the η^3-butenyl–Ni^{II} and the $\eta^1(C^1)$-butenyl–Ni^{II} bond along the most feasible pathway, $k_1(\pi)$ and $k_1(\sigma)$, respectively. This has been confirmed by free optimizations following the imaginary eigenmode downhill from slightly relaxed structures of **3π** and **3σ**, respectively. The $\eta^1(C^3)$-butenyl species, **2σ′**, can be considered to be the precursor for two different elementary processes: i) *anti*–*syn* isomerization via **5** and, ii) *cis*-butadiene insertion into the $\eta^1(C^3)$-butenyl–Ni^{II} bond. The latter process gives rise to 1,2-polymer units with C^1–C^3 linkages (according to the σ-allyl insertion mechanism). The catalytic cycle for the generation of 1,2-polybutadienes, however, is not considered in the present study, and will be the subject of a forthcoming investigation.

cis-Butadiene insertion into the $\eta^1(C^1)$-σ-butenyl–Ni^{II} bond: Several routes for this process were tested. The most feasible pathway for *cis*-butadiene insertion into the $\eta^1(C^1)$-butenyl–Ni^{II} bond proceeds via a SPY transition state structure that consists of a quasiplanar four-membered *cis* arrangement of the double bond in the inserting butadiene molecule, the $\eta^1(C^1)$-butenyl group, and of the nickel atom. The skeletal rearrangements involved along the most likely pathway are schematically depicted in Figure 5. Commencing from the

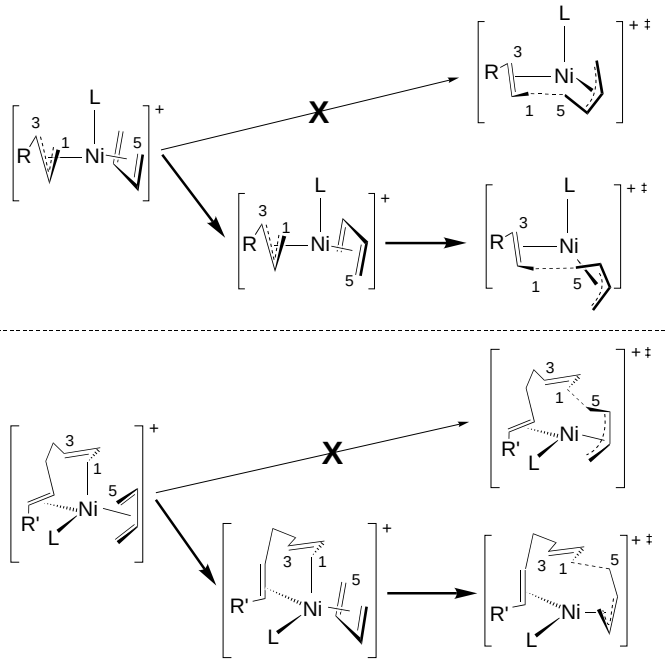

Figure 5. Skeletal rearrangements along the most feasible pathway for the monomer insertion step to occur by *cis*-butadiene insertion into the η^3-π-butenyl–Ni^{II} bond (top) or into the $\eta^1(C^1)$-σ-butenyl–Ni^{II} bond (bottom). (Exemplified for the *syn*-butenyl form).

TBPY species, **2σ**, the C–C bond formation proceeds through the SPY transition state **3σ**, where the apical $\eta^1(C^1)$-butenyl–Ni^{II} bond and the *cis*-oriented η^4-*cis*-butadiene double bond are nearly coplanar. In this process, *cis*-butadiene and the growing chain's coordinating double bond undergo rotation, with the $\eta^1(C^1)$-butenyl group acting as the pivot. After reaching **3σ**, the coordination of the polybutadienyl chain is cleaved to form the SP *anti*-η^3-butenyl product **4a**. We have not been able to locate the transition state for the TBPY → SPY skeletal rearrangements. However, free optimizations following the imaginary eigenmode downhill from slightly relaxed structures of **3σ** towards **2σ** give no indications of a significant kinetic barrier associated with skeletal

rearrangements. In contrast, butadiene insertion via a TBPY transition-state structure (i.e., without skeletal rearrangements involved) is not a viable pathway because it is associated with a significantly higher barrier.

The analysis of the electronic structure of **3σ** and **3π**, as exemplified in Table 2 for *syn*-butenyl forms, provides interesting insights into the difference of the electronic nature for the monomer insertion along the alternative $k_1(\sigma)$ and $k_1(\pi)$ routes. What is similar to both paths is the observation that the electron density on the C^1 and C^5 carbons of the emerging C–C bond decreases in **3** when compared to **2**. The polarity of the two reacting terminal carbons, however, is quite different in **3σ** and **3π**. On the one hand, the two carbons carry a very similar electron density in **3π**, giving rise to an overall small positive charge on the reactive centers. In contrast, **3σ** is characterized by a distinct accumulation of electron density on the reactive carbons, with the terminal butenyl-C^1 carbon carrying a notable negative charge. Overall, the differences in the electronic properties of the monomer insertion step along $k_1(\sigma)$ and $k_1(\pi)$ is attributed to the polarity of the butenyl–Ni^{II} bond. For both **2** and **3**, the butenyl–Ni^{II} bond is found to be more polar for the $\eta^1(C^1)$-mode relative to the η^3-coordination mode.

The distinct electronic character of the insertion process taking place along $k_1(\sigma)$ and $k_1(\pi)$ is also reflected in the geometries of the transition-state structures. In contrast to the product-like **3π**,[7b] *cis*-butadiene insertion into the more polar $\eta^1(C^1)$-butenyl–Ni^{II} bond occurs at an earlier stage of the process through an educt-like transition state **3σ** that is characterized by a surprisingly large distance of ≈2.40 Å of the C–C bond being formed.

The enthalpy gap between *anti* and *syn* forms in **2σ** is preserved in **3σ**. Accordingly, the intrinsic insertion enthalpies are very similar for the $k_{1c}(\sigma)$ and $k_{1t}(\sigma)$ pathways and amount to 12.6 kcal mol^{-1} ($\Delta H_{int}^{\neq}{}_{1c(\sigma)}$, **2aσ** → **3aσ**)[34] and to 12.4 kcal mol^{-1} ($\Delta H_{int}^{\neq}{}_{1t(\sigma)}$, **2sσ** → **3sσ**),[34] respectively (Table 1). This indicates a nearly identical intrinsic reactivity of the *anti*- and *syn*-$\eta^1(C^1)$ forms, which is in contrast to the different reactivity of the two isomeric η^3-butenyl forms.[7b, 6e]

cis-Butadiene insertion into the η^3-π-butenyl–Ni^{II} bond: For purposes of comparison, we summarize in this section the most important aspects of this process. The *cis*-butadiene insertion into the η^3-butenyl–Ni^{II} bond preferentially occurs via a TBPY transition-state structure, composed of a quasi-planar four-membered arrangement of the terminal butenyl-C^1, the double bonds of the inserting butadiene, and by the nickel atom in the equatorial coordination plane. This entails skeletal rearrangements from the formally 18 e$^-$ SPY η^3-butenyl η^4-*cis*-butadiene species **2π** to the TBPY transition state **3π** and from there to the formally 16 e$^-$ quasi square-planar (SP) *anti*-η^3-butenyl product **4a** (Figure 5). Consequently, prone butadiene forms are distinctly more reactive than supine butadiene forms. This is because the insertion commencing from the thermodynamically most stable supine η^4-*cis*-butadiene isomers via a SPY transition state (i.e., without skeletal rearrangements involved), a quasiplanar arrangement of the reactive parts is precluded, giving rise to an insurmountable barrier (>30 kcal mol^{-1} ΔH).[7b]

The activation enthalpy for *cis*-butadiene insertion into the *anti*- and *syn*-η^3-butenyl–Ni^{II} bond amounts to 16.6 kcal mol^{-1} ($\Delta H^{\neq}{}_{1c(\pi)}$, **2aπ** → **3aπ**)[34] and 15.3 kcal mol^{-1}($\Delta H^{\neq}{}_{1t(\pi)}$, **2sπ** → **3sπ**),[34] respectively (Table 1). Therefore, the thermodynamically more stable *syn*-butenyl isomer **2sπ** must be regarded as also more reactive than the *anti* isomer **2aπ**. Additionally, the kinetic barriers are found to be almost unaffected by the enantioface of the butenyl group involved in the insertion process, as indicated by very similar barriers for supine and prone butenyl isomers (Table 1).

anti–syn Isomerization: The interconversion of the two isomeric forms of the η^3-butenyl–transition metal bond is most likely to take place by means of a η^3-π → $\eta^1(C^3)$-σ butenyl group conversion, followed by internal rotation of the vinyl group around the C^2–C^3 single bond. This has been confirmed both by experimental[35] and theoretical[19] evidence.

A TBPY transition state, **5**, is passed through for isomerization along the most feasible pathway, which consists of the internal rotation of the vinyl group around the formal C^2–C^3 single bond. We have located several isomers of **5** in which the $\eta^1(C^3)$-butenyl group occupies an axial position. The energetics for the energetically favored isomer are included in Table 1. Following the reaction path downhill to both sides in free optimizations starting from slightly distorted structures of **5** shows that **2σ′** is the direct precursor for isomerization.

For a facile isomerization, we found that both **2σ′** and **5** must be stabilized by a saturated ligand sphere around Ni^{II}. Therefore, the coordination number of Ni^{II} must always be kept at five during isomerization. *cis*-Butadiene, as well as the growing polybutadienyl chain, are both likely to participate in the isomerization process by coordination to the nickel atom. Investigations on model systems in which *cis*-butadiene was substituted by two ethylenes, to represent the coordination of additional double bonds from the growing polybutadienyl chain, revealed that the latter could not compete energetically with *cis*-butadiene coordination.

Therefore, it is most probable that isomerization takes place in **2** when commencing from the *anti*-η^3-butenyl species **2aπ**, followed by rearrangement into **2aσ′**, subsequent rotational isomerization via the $\eta^1(C^3)$ transition state **5** that gives **2sσ′** which rearranges into the thermodynamically more stable η^3-*syn* isomer **2sπ**. The intrinsic activation enthalpy for *anti–syn* isomerization amounts to 6.8 kcal mol^{-1} ($\Delta H_{int}^{\neq}{}_{iso}$, **2aσ′** → **5**)[34] while a barrier of 21.4 kcal mol^{-1} ($\Delta H^{\neq}{}_{iso}$, **2aπ** → **5**) must be overcome relative to the most stable *anti* isomer **2aπ**.

Thermochemical reaction profile: The condensed thermochemical profile for the *trans*-1,4 (along k_{1t}) and *cis*-1,4 (along k_{1c}) production cycle for the catalyst model **I** is given in Figure 4. It consists of *cis*-butadiene insertion into the $\eta^1(C^1)$-butenyl–Ni^{II} bond and the η^3-butenyl–Ni^{II} bond as well as *anti–syn* isomerization. From this profile it is evident that for *cis*-butadiene insertion along $k_1(\sigma)$ a distinctly higher activation barrier ($\Delta\Delta H^{\neq} = 6.6$ kcal mol^{-1} for $k_{1t}(\sigma)$ relative to $k_{1t}(\pi)$)[34] must be overcome than along $k_1(\pi)$. This corroborates our previous conclusion,[7] that the monomer insertion step is most likely to proceed by *cis*-butadiene insertion into

  0947-6539/02/0820-4762 $ 20.00+.50/0 *Chem. Eur. J.* **2002**, *8*, No. 20

the η^3-butenyl–Ni^{II} bond. However, $\eta^1(C^1)$-butenyl–Ni^{II} species, although they are commonly believed to be reactive intermediates, are predicted to be sparsely populated and also to be distinctly less reactive than η^3-butenyl–Ni^{II} species. Therefore, $\eta^1(C^1)$ species are not likely to be involved along viable pathways for *cis*-butadiene insertion into the butenyl–Ni^{II} bond. This clearly indicates that the π-allyl insertion mechanism is the favorable mechanism for the monomer insertion step in the allylnickel(II)-catalyzed 1,4-polymerization of 1,3-butadiene, while the proposed alternative σ-allyl insertion mechanism must be considered as not operative. In the discussions below, we shall elaborate further on the implications for the mechanism of stereoregulation.

Catalyst model II: Among the number of isomeric forms possible for each species, most of which have been carefully explored, only the most stable isomers are reported. Similar to our investigation for model **I**, isomers were explicitly considered here that originate from the two enantiomeric forms of the *cis*-butadiene – Ni^{II} coordination and the butenyl – Ni^{II} coordination, for both *anti*- and *syn*-butenyl forms. Table 3 summarizes the free energies (ΔG, ΔG^{+}) of key stationary points along the most feasible pathway of competing routes for crucial elementary steps. The condensed Gibbs free-energy profile of the catalytic cycle is presented in Figure 6. The geometric and electronic features of critical elementary steps of the overall polymerization cycle have been analyzed in detail for the catalyst model **I**. Therefore, we shall focus the discussion of the catalyst model **II** on energetic aspects.

Butadiene π-complex: As regards the π-butenyl species **2π**, they are found to be very similar for catalyst models **I** and **II**, respectively. In both cases, **2π** is the thermodynamically most stable form of **2**, with *cis*-butadiene preferentially coordinating in a supine-η^4 fashion. With regard to the most stable isomers, the *syn*-butenyl form **2Sπ** is 2.4 kcal mol^{-1} lower in energy than the *anti* form **2Aπ**, respectively (ΔG),[34] which is very similar to that found for model **I** ($\Delta H = 2.7$ kcal mol^{-1}).

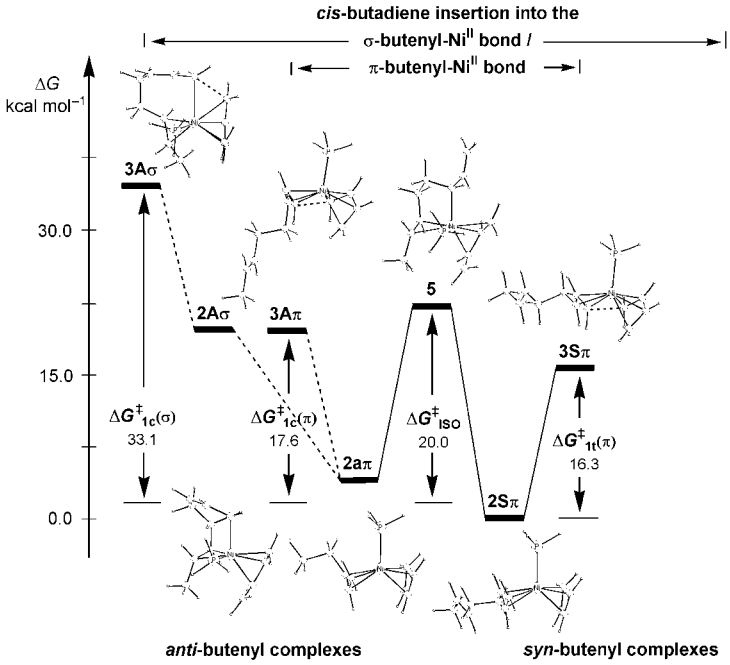

Figure 6. Condensed free-energy profile (ΔG, ΔG^{+}[kcal mol^{-1}]) of competitive pathways for the generation of *trans*-1,4 (——, along k_{1t}) and *cis*-1,4 (- - - -, along k_{1c}) polymer units for the $[(C_8H_{13})Ni^{II}(cis\text{-}C_4H_6)PH_3]^+$ catalyst model **II**, consisting of *cis*-butadiene insertion into the $\eta^1(C^1)$-σ- and the η^3-π-butenyl – Ni^{II} bond and of *anti* – *syn* isomerization.

The chelating polybutadienyl chain, however, substantially influences the stability and reactivity of **2σ**. Despite numerous attempts, we have not been able to locate the *syn*-$\eta^1(C^1)$ form, **2Sσ**. This might caused by the prohibitively large steric strain associated with incorporation of a *trans* double bond in a seven-membered chelate ring, where the C^1 and C^6, C^7 carbons occupy axial and equatorial positions, respectively, in the TBPY **2σ**. The stability of the *anti* $\eta^1(C^1)$ form, **2Aσ**, is also found to be highly affected by steric strain. The energetic gap between *anti*-η^3 and -$\eta^1(C^1)$ species, **2Aπ** and **2Aσ**, respectively, increases to 17.7 kcal mol^{-1} (ΔG),[34] which is ≈9.5 kcal mol^{-1} higher, than the results obtained for model **I**. However, it is unlikely that the five-membered chelate ring in **2σ′** imposes any serious steric strain. Thus the thermodynamic stability of **2σ′** remains essentially unaffected upon coordination of the first double bond of the growing polymer chain to nickel. This is indicated by a very similar stability of corresponding isomers for catalyst models **I** and **II**, respectively. Again, both *anti*- (**2Aσ′**) and *syn*- (**2Sσ′**) butenyl isomers as well as the two enantiomeric *Re*/*Si*-butenyl forms for each of them are found to be very close in energy. As a consequence of the different extents of steric strain associated with the chelate rings in **2σ** and **2σ′**, respectively, the $\eta^1(C^3)$-butenyl species, **2σ′**, becomes thermodynamically more stable by 1.8 kcal mol^{-1} (ΔG)[34] relative to **2σ** for *anti* forms. This is in contrast to the reverse order of thermodynamic stability, between **2σ** and **2σ′**, found for the catalyst model **I**.

Table 3. Calculated Gibbs free energy profile for crucial steps of the polymerization cycle for the $[(C_8H_{13})Ni^{II}(cis\text{-}C_4H_6)PH_3]^+$ catalyst model **II**.[a–d]

Category	Description[b]	Species	ΔG, ΔG^{+} [kcal mol^{-1}][c]
cis-butadiene	*syn*-η^3-butenyl (*S*/*P*)	**2Sπ**	0.0/2.8
π-complex	*anti*-η^3-butenyl (*S*/*P*)	**2Aπ**	2.4/6.3
	syn-$\eta^1(C^1)$-butenyl (*Re*/*Si*)	**2Sσ**	–
	anti-$\eta^1(C^1)$-butenyl (*Re*/*Si*)	**2Aσ**	20.0/20.2
	syn-$\eta^1(C^3)$-butenyl (*Re*/*Si*)	**2Sσ′**	17.9/18.2
	anti-$\eta^1(C^3)$-butenyl (*Re*/*Si*)	**2Aσ′**	18.5/18.1
insertion TS	*syn*-η^3-butenyl (*S*/*P*)	**3Sπ**	16.5/16.1
	anti-η^3-butenyl (*S*/*P*)	**3Aπ**	19.8/20.2
	syn-$\eta^1(C^1)$-butenyl (*Re*/*Si*)	**3Sσ**	–
	anti-$\eta^1(C^1)$-butenyl (*Re*/*Si*)	**3Aσ**	35.7/35.2
	anti-$\eta^1(C^3)$-butenyl (*Re*/*Si*)[d]	**Aσ′**	32.5/32.1
isomerization TS		**5**	22.0

[a] Only the most stable isomer for each species is reported. The two enantiomeric forms for both the *anti*- and *syn*-butenyl – Ni^{II} coordination (cf. Figure 3) are explicitly given for the energetically favored *cis*-butadiene orientation (see text). [b] The enantiomers of the butenyl – Ni^{II} coordination are denoted in the following way. The notation given in parenthesis refers to supine (*S*) or prone (*P*) for η^3-butenyl – Ni^{II} species and to *Re* or *Si* for η^1-butenyl – Ni^{II} species (cf. Figure 3). [c] Gibbs free energies relative to $[(syn\text{-}\eta^3\text{-}C_8H_{13})Ni^{II}(\eta^4\text{-}cis\text{-}C_4H_6)PH_3]^+$ **4Sπ**. [d] The transition-state structure **3Aσ′** for *cis*-butadiene insertion into the *anti*-$\eta^1(C^3)$-butenyl – Ni^{II} bond (not shown in Scheme 1) is included for comparison.

cis-Butadiene insertion into the η^3-π-butenyl–Ni^{II} bond and into the η^1-σ-butenyl–Ni^{II} bond: For *cis*-butadiene insertion into the η^3-butenyl–Ni^{II} bond, activation barriers were obtained that were very similar to those reported above. The thermodynamically more stable *syn*-η^3-butenyl form is also predicted to be more reactive than the *anti* form, since the free energy of activation for *cis*-butadiene insertion into the *syn*-η^3-butenyl–Ni^{II} bond and the *anti*-η^3-butenyl–Ni^{II} bond differ by 1.3 kcal mol^{-1} ($\Delta G^{\neq}_{1t(\pi)} = 16.3$ kcal mol^{-1}, **2Sπ** → **3Sπ**; $\Delta G^{\neq}_{1c(\pi)} = 17.6$ kcal mol^{-1}, **2Aπ** → **3Aπ**, respectively)[34] with the *syn* form having the lower barrier. Nearly identical kinetic barriers were obtained for $k_{1t(\pi)}$ and $k_{1c(\pi)}$, respectively, regardless of which butenyl enantioface is involved in the insertion process (Table 3).

In contrast to the findings for the monomer insertion step along $k_1(\pi)$, the activation barriers for *cis*-butadiene insertion into the $\eta^1(C^1)$-butenyl–Ni^{II} bond are affected to a large extent by the coordination of the chelating polybutadienyl chain. The intrinsic free-energy barrier for *anti* forms ($\Delta G_{int}{}^{\neq}_{1c(\sigma)}$ = **2Aσ** → **3Aσ**)[34] increases to 17.2 kcal mol^{-1}, which is ≈5 kcal mol^{-1} higher than the enthalpic barrier for the **2aσ** → **3aσ** process. This is due to the destabilization of **3Aσ** relative to **2Aσ**, caused by the higher steric strain associated with the seven-membered chelate ring in **3Aσ**, that arises from the skeletal rearrangements involved along the monomer insertion step (cf. Figure 5). In terms of total free-energy barriers, relative to the most stable isomer of **2Aπ**, the two alternative routes for the monomer insertion step along either $k_{1c}(\sigma)$ or $k_{1c}(\pi)$ have a distinct separation of 15.5 kcal mol^{-1} ($\Delta G^{\neq}_{1c(\pi)} = 17.6$ kcal mol^{-1}, **2Aπ** → **3Aπ**; $\Delta G^{\neq}_{1c}(\sigma) = 33.1$ kcal mol^{-1}, **2Aπ** → **3Aσ**, respectively). This leads us to conclude that i) in agreement with the findings for model **I**, *cis*-butadiene insertion into the η^3-butenyl–Ni^{II} bond has to be considered as the kinetically favored route for the monomer insertion step, and ii) the distinctly less reactive $\eta^1(C^1)$-butenyl species are precluded from the most feasible pathway.

Although we are primarily concerned here with the stereoselective 1,4-polymerization of butadiene, we have also probed the *cis*-butadiene insertion for the thermodynamically more stable $\eta^1(C^3)$-butenyl species **2σ′**. For *cis*-butadiene insertion into the *anti*-$\eta^1(C^3)$-butenyl–Ni^{II} bond, we found a free-energy of activation that is 3.2 kcal mol^{-1} lower than for insertion into the *anti*-$\eta^1(C^1)$-butenyl–Ni^{II} bond ($\Delta G^{\neq} = 29.9$ and 33.1 kcal mol^{-1} for the **2Aπ** → **3Aσ′** and **2Aπ** → **3Aσ** processes, respectively).[34] This indicates a higher reactivity of the thermodynamically more stable **2σ′** species relative to **2σ**. Consequently, provided that the σ-allyl insertion mechanism is operative, a 1,2-polybutadiene is suggested to be formed as the predominant product. Furthermore, the 1,2-polybutadiene should lack any stereoregularity within the vinyl groups (atactic polymer structure), since nearly identical barriers are predicted for the two enantiomeric *Re*/*Si*-$\eta^1(C^3)$ forms. This clearly contradicts with experiment and provides further evidence that the σ-allyl insertion mechanism is not operative.

anti–syn Isomerization: Among the several possible isomers of the TBPY transition state, **5**, for *anti–syn* isomerization, most of which we have carefully scrutinized, the isomer that preferentially passes along the minimum energy pathway is 19.6 kcal mol^{-1} higher in free-energy relative to **2Aπ** ($\Delta G^{\neq}_{iso}$, **2Aπ** → **5**). The chelating polybutadienyl chain is seen to decrease the activation barrier for *anti–syn* isomerization, since the barrier is lower than that for the catalyst model **I** (see above).

Interrelation of kinetic barriers for monomer insertion and *anti–syn* isomerization—implications for the mechanism of *cis–trans* regulation: This section is devoted to the implications of the nature of the monomer insertion step on the mechanism of *cis–trans* regulation. As regards the π-allyl insertion mechanism, we shall start with a brief summary of crucial aspects in order to understand the high *trans*-1,4 selectivity of the catalyst under investigation. This has previously been presented for the $[(C_8H_{13})Ni^{II}(cis\text{-}C_4H_6)P(OMe)_3]^+$ model catalyst;[8] the condensed free-energy profile is provided in the Supporting Information (Figure S1).

For *cis*-butadiene insertion into the η^3-butenyl–Ni^{II} bond, the thermodynamically more stable *syn* form is predicted to also be more reactive than the *anti* form (i.e., $k_{1t}(\pi) > k_{1c}(\pi)$). A facile *anti–syn* isomerization is indispensable for making the *trans*-1,4-polymer generating cycle along $k_{1t}(\pi)$ accessible (Scheme 1). The barrier for isomerization ($\Delta G^{\neq}_{iso}$) is higher than the insertion barrier along the *trans*-1,4-polymer generating cycle ($\Delta G^{\neq}_{1t}(\pi)$), but lower than the activation barrier associated with the *cis*-1,4-polymer generating cycle ($\Delta G^{\neq}_{1c}(\pi)$, Figure S1). This would indicate that isomerization can be considered to be facile enough to make the $k_{1t}(\pi)$ pathway accessible, while the competing $k_{1c}(\pi)$ pathway remains almost completely suppressed because of the lesser reactivity of *anti*-η^3-butenyl form when compared to the *syn* form ($k_{1t}(\pi) > k_{iso} > k_{1c}(\pi)$). Consequently, in the presence of butadiene, the less reactive *anti* form should be enriched in the reaction solution, while the thermodynamically more stable *syn* form practically does not exist in a detectable amount because of its higher reactivity. A polybutadiene of predominantly *trans*-1,4 structure should be formed and *anti–syn* isomerization has to be considered as the rate-determining step of the entire polymerization cycle. All these aspects are consistent with experimental observations.[6e]

Although nearly identical intrinsic barriers are found for *cis*-butadiene insertion into the *anti*- and *syn*-η^1-butenyl–Ni^{II} bond for catalyst model **I** (relative to **2aσ** and **2sσ**, respectively), in terms of total barriers (relative to most stable *anti* and *syn* isomer of **2**, namely **2aπ** and **2sπ**, respectively) our calculations indicate a higher reactivity of the thermodynamically less stable *anti*-η^1-butenyl form relative to the thermodynamically more stable *syn*-η^1-butenyl form (20.5 and 21.9 kcal mol^{-1} for $\Delta H^{\neq}_{1c}(\sigma)$, **2aπ** → **3aσ′**, and $\Delta H^{\neq}_{1t}(\sigma)$, **2sπ** → **3sσ′**, respectively; cf. Figure 4).[34] Therefore, regardless of whether *anti–syn* isomerization is slower or more rapid relative to *cis*-butadiene insertion, a polybutadiene of predominantly *cis*-1,4 structure should always be formed if monomer insertion follows the $k_1(\sigma)$ route. For catalyst model **II** with the chelating polybutadienyl chain, the relative stability and reactivity between $\eta^1(C^1)$- and $\eta^1(C^3)$-butenyl species is predicted to be reversed, with $\eta^1(C^3)$ forms becoming more favored. This would suggest that a polybuta-

0947-6539/02/0820-4764 $ 20.00+.50/0 *Chem. Eur. J.* **2002**, *8*, No. 20

diene of predominantly 1,2-structure should be formed for monomer insertion along the $k_1(\sigma)$ route. This leads us to conclude that the kinetically disabled σ-allyl insertion mechanism does not provide a reasonable understanding of the *cis*–*trans* selectivity and the chemoselectivity in the allylnickel(II)-catalyzed 1,4-polymerization of 1,3-butadiene.

Conclusion

We have presented a theoretical investigation on the nature of the monomer insertion step in the allylnickel(II)-catalyzed 1,4-polymerization of 1,3-butadiene that employed a gradient-corrected DFT-method aimed at elucidating the similarities and differences between the two mechanistic proposals for the monomer insertion step in the transition metal-catalyzed 1,4-polymerizaion of 1,3-butadiene. These proposals are the σ-allyl insertion mechanism of Cossee/Arlman[10] and the π-allyl insertion mechanism suggested by Taube et al.[13] We have investigated *cis*-butadiene insertion into either the η^1-σ-butenyl–Ni^{II} bond (σ-allyl insertion mechanism along $k_1(\sigma)$) following competing pathways to generate *trans*-1,4 and *cis*-1,4 polymer units and also *anti*–*syn* isomerization for two catalyst models of the *trans*-1,4 regulating $[RC_3H_4Ni^{II}(C_4H_6)L]^+$ catalyst; namely $\{[(C_4H_7)Ni^{II}(cis\text{-}C_4H_6)PH_3]^+ (+C_2H_4)\}$, **I**, and $[(C_8H_{13})Ni^{II}(cis\text{-}C_4H_6)PH_3]^+$, **II**. We have provided a detailed insight and understanding of the different nature of the monomer insertion step according to the two mechanistic alternatives and we have shown why the π-allyl insertion mechanism is favored over the σ-allyl insertion mechanism.

The thermodynamically most stable η^1-butenyl and η^3-butenyl forms of **2** arise from *cis*-butadiene coordination in a bidentate fashion (η^4-*cis*-butadiene). **2π** and **2σ** represent the direct precursor structures for *cis*-butadiene insertion into the η^3-butenyl–Ni^{II} bond following the $k_1(\pi)$ route and into the $\eta^1(C^1)$-butenyl–Ni^{II} bond following $k_1(\sigma)$, respectively. They are energetically well-separated. **2π** is thermodynamically strongly preferred, while **2σ** should be sparsely populated. The gap between η^3-butenyl and η^1-butenyl species becomes increased by the chelating polybutadienyl chain as a result of steric strain associated with the formation of the seven-membered ring. The *syn* forms are thermodynamically more stable than the *anti* forms for both **2π** and **2σ**. The *syn*–*anti* gap, however, is less pronounced for the η^1-mode relative to the η^3-mode of the butenyl–Ni^{II} coordination.

cis-Butadiene insertion into the η^3-butenyl–Ni^{II} as well as into the $\eta^1(C^1)$-butenyl–Ni^{II} bond entails skeletal rearrangements along the most feasible pathway. SPY and TBPY transition-state structures, **3σ** and **3π**, are passed through along $k_1(\sigma)$ and $k_1(\pi)$, respectively, which are characterized by a quasiplanar four-membered arrangement of the reactive parts, namely the terminal butenyl-C^1, the double bond of the inserting butadiene and the nickel atom. The orientation of *cis*-butadiene is fixed in the insertion transition states, whereas the enantioface of the butenyl group involved in the insertion process has a minor influence on the kinetic barrier in the absence of steric crowding.

The monomer insertion step along $k_1(\pi)$ and $k_1(\sigma)$, respectively, exhibits a different electronic character as a consequence of the higher polarity of the η^1-butenyl–Ni^{II} bond compared to that of the η^3-coordination mode. This gives rise to a product-like transition state, **3π**, along $k_1(\pi)$, whereas an educt-like transition state, **3σ**, is passed through along $k_1(\sigma)$.

The intrinsic reactivity of the isomeric *anti*- and *syn*-butenyl forms is shown to be different along the $k_1(\sigma)$ and $k_1(\pi)$ routes for monomer insertion. Nearly identical intrinsic insertion barriers were obtained for the two forms along $k_1(\sigma)$, thus indicating a very similar intrinsic reactivity of *anti*- and *syn*-$\eta^1(C^1)$-butenyl forms. In contrast, a different intrinsic reactivity of *anti*- and *syn*-η^3-butenyl forms can be assumed from the insertion barriers along $k_1(\pi)$, with the η^3-*syn* form expected to be more reactive than its η^3-*anti* counterpart.

anti–*syn* isomerization is most likely to proceed by means of a $\eta^3 \rightarrow {}^1(C^3)$ conversion of the butenyl group, followed by internal rotation of the vinyl group around the C^2–C^3 single bond via a TBPY $\eta^1(C^3)$-transition state. *cis*-Butadiene as well as the coordinating polybutadienyl chain have to participate in the most feasible pathway of this process.

For *cis*-butadiene insertion into the $\eta^1(C^1)$-butenyl–Ni^{II} bond, a distinctly higher activation barrier has to be overcome relative to the insertion into the η^3-butenyl–Ni^{II} bond. Thus the thermodynamically more stable and more highly populated η^3-butenyl species also appear as more reactive than the corresponding η^1-butenyl species. The difference in stability and reactivity between η^3-π and η^1-σ species is shown to increase under the influence of steric strain imposed by the chelating polybutadienyl chain. The sparsely populated and distinctly less reactive η^1-σ-butenyl species, although they are commonly believed to be reactive intermediates, are not likely to be involved along feasible pathways for monomer insertion. This corroborates our previous conclusion,[7] that the π-allyl insertion mechanism represents the preferred mechanism for the monomer insertion step in the allylnickel(II)-catalyzed 1,4-polymerization of 1,3-butadiene, for both thermodynamic and kinetic reasons. The alternatively proposed σ-allyl insertion mechanism has to be considered as being not operative.

The *cis*–*trans* regulation is elucidated in a consistent way with preferential insertion of *cis*-butadiene into the η^3-butenyl–Ni^{II} bond. In contrast, monomer insertion according to the σ-allyl insertion mechanism would neither provide a rationalization of *cis*–*trans* selectivity nor of chemoselectivity in the allylnickel(II)-catalyzed 1,4-polymerization of 1,3-butadiene.

Acknowledgments

The author is grateful to Prof. Dr. Rudolf Taube for valuable and stimulating discussions and for his ongoing interest on this research. The author is furthermore indebted to Prof. Dr. Reinhart Ahlrichs (University of Karlsruhe, Germany) for making the latest version of TURBOMOLE available. Excellent service by the computer centers URZ Halle and URZ Magdeburg is gratefully acknowledged.

[1] R. T. La Flair, U. U. Wolf in *Ullmann's Encyclopedia of Industrial Chemistry*, *5th ed.*, *Vol. A23*, Verlag Chemie, Weinheim, Germany, **1993**, pp. 273–282.

[2] a) *Applied Homogeneous Catalysis with Organometallic Complexes* (Eds.: B. Cornils, W. A. Herrmann), VCH, Weinheim, Germany, **1996**; b) L. Porri, A. Giarrusso in *Comprehensive Polymer Science*, *Vol. 4* (Eds.: G. C. Eastmond, A. Ledwith, S. Russo, B. Sigwalt), Pergamon, Oxford (UK), **1989**, Part II, pp. 53 – 108.

[3] a) P. Teyssie, M. Julemont, J. M. Thomassin, E. Walkiers, R. Warin in *Coordination Polymerization* (Eds.: J. C. W. Chien), Academic Press, New York, **1975**, pp. 327 – 347; b) J. Boor, Jr. in *Ziegler-Natta Catalysts and Polymerizations*, Academic Press, New York, **1979**; c) L. Porri in *Structural Order in Polymers* (Eds.: F. Ciardelli, P. Giusti), Pergamon Press, Oxford (UK), **1981**, pp. 51 – 62.

[4] a) M. I. Lobach, V. A. Kormer, I. Yu. Tsereteli, G. P. Kondoratenkov, B. D. Babitskii, V. I. Klepikova, *J. Polym. Sci. Polym. Lett.* **1971**, *9*, 71; b) R. Warin, P. Teyssié, P. Bourdaudurq, F. Dawans, *J. Polym. Sci. Polym. Lett.* **1973**, *11*, 177.

[5] a) V. A. Kormer, B. D. Babitskii, M. I. Lobach, *Adv. Chem. Series* **1969**, *91*, 306; b) B. A. Dolgoplosk, S. I. Beilin, Yu. V. Korshak, K. L. Makovetsky, E. I. Tinyakova, *J. Polym. Sci. Polym. Chem. Ed.* **1973**, *11*, 2569; c) P. W. Jolly, G. Wilke, *The Organic Chemistry of Nickel*, *Vol. 2*, *Organic Synthesis*, Academic Press, New York, **1975**.

[6] a) J. F. Harrod, L. R. Wallace, *Macromolecules* **1969**, *2*, 449; b) R. P. Hughes, J. Powell, *J. Am. Chem. Soc.* **1972**, *94*, 7723; c) N. N. Druz, A. V. Zak, M. I. Lobach, V. A. Vasiliev, V. A. Kormer, *Eur. Polym. J.* **1978**, *14*, 21; d) R. Warin, M. Julemont, P. Teyssie, *J. Organomet. Chem.* **1980**, *185*, 413; e) R. Taube, J.-P. Gehrke, R. Radeglia, *J. Organomet. Chem.* **1985**, *291*, 101; f) R. Taube, S. Wache, *J. Organomet. Chem.* **1992**, *428*, 431; g) R. Taube, S. Wache, J. Sieler, *J. Organomet. Chem.* **1993**, *459*, 335.

[7] a) S. Tobisch, H. Bögel, R. Taube, *Organometallics* **1996**, *15*, 3563; b) S. Tobisch, H. Bögel, R. Taube, *Organometallics* **1998**, *17*, 1177; c) S. Tobisch, R. Taube, *Organometallics* **1999**, *18*, 5204; d) S. Tobisch, R. Taube, *Chem. Eur. J.* **2001**, *7*, 3681.

[8] S. Tobisch, *Acc. Chem. Res.* **2002**, *35*, 96.

[9] P. Pino, U. Giannini, L. Porri in *Encyclopedia of Polymer Science and Engineering*, *2nd ed.*, *Vol. 8*, Wiley, New York, **1987**, pp. 147 – 220.

[10] a) P. Cossee in *Stereochemistry of Macromolecules*, *Vol. 1* (Ed.: A. D. Ketley), Marcel Dekker, New York, **1967**, p. 145; b) E. J. Arlman, *J. Catal.* **1966**, *5*, 178.

[11] a) H. Lehmkuhl, T. Keil, R. Benn, A. Rufinska, C. Krüger, J. Poplawska, M. Bellenbaum, *Chem. Ber.* **1988**, *121*, 1931; b) C. A. Tolman, *J. Am. Chem. Soc.* **1970**, *92*, 6777.

[12] a) L. Porri, A. Giarrusso, G. Ricci, *Polym. Sci. Ser. A* **1994**, *36*, 1421; b) A. Peluso, R. Improta, A. Zambelli, *Organometallics* **2000**, *19*, 411.

[13] a) R. Taube, J.-P. Gehrke, P. Böhme, *Wiss. Zeitschr. Tech. Hochschule Leuna-Merseburg* **1987**, *39*, 310; b) R. Taube, U. Schmidt, J.-P. Gehrke, P. Böhme, J. Langlotz, S. Wache, *Makromol. Chem. Makromol. Symp.* **1993**, *66*, 245; c) R. Taube, G. Sylvester in *Applied Homogeneous Catalysis with Organometallic Complexes* (Eds.: B. Cornils, W. A. Herrmann), VCH, Weinheim, Germany, **1996**, pp. 280 – 317.

[14] a) S. Lieber, M.-H. Prosenc, H.-H. Brintzinger, *Organometallics* **2000**, *19*, 377; b) P. M. Margl, T. K. Woo, T. Ziegler, *Organometallics* **1998**, *17*, 4997.

[15] S. Tobisch, unpublished results.

[16] The olefin insertion can also favorably take place into the η^1-σ-allyl – transition metal bond, as a result of a conformational preference of the η^1-σ relative to the η^3-π coordination mode; see for example, M. Dahlmann, G. Erker, K. Bergander, *J. Am. Chem. Soc.* **2000**, *122*, 7986.

[17] This rate law has been derived with respect to the [(η^3-butenyl)$Ni^{II}L_2$] precatalyst **1**, which therefore includes the K_1 substitution step.

[18] a) *Mechanisms in Inorganic Chemistry* (Eds.: F. Basolo, R. G. Pearson), Thieme, Stuttgart, Germany, **1973**; b) M. L. Tobe in *Comprehensive Coordination Chemistry*, *Vol. I* (Eds.: G. Wilkinson, R. D. Gillard, J. A. McCleverty), Pergamon Press, New York, **1987**, pp. 281 – 384; c) R. J. Cross, *Chem. Soc. Rev.* **1985**, *14*, 197; d) R. J. Cross, *Adv. Inorg. Chem.* **1989**, *34*, 219.

[19] S. Tobisch, R. Taube, *Organometallics* **1999**, *18*, 3045.

[20] a) An ethylene ligand was chosen as a simplified model for the coordination of the second or any further double bond of the polybutadienyl chain because of the high conformational flexibility of the polybutadienyl chain, consisting of three or more C_4 units. b) The coordinating first double bond of the growing polybutadienyl chain arises from the ultimate inserted C_4 unit as achieved in the insertion products **4**.

[21] V. A. Kormer, M. I. Lobach, V. I. Klepikova, B. D. Babitskii, *J. Polym. Sci. Polym. Lett.* **1976**, *14*, 317.

[22] R. Taube, J.-P. Gehrke, P. Böhme, J. Köttnitz, *J. Organomet. Chem.* **1990**, *395*, 341.

[23] a) M. Häser, R. Ahlrichs, *J. Comput. Chem.* **1989**, *10*, 104; b) R. Ahlrichs, M. Bär, M. Häser, H. Horn, C. Kölmel, *Chem. Phys. Lett.* **1989**, *162*, 165.

[24] a) P. A. M. Dirac, *Proc. Cambridge Philos. Soc.* **1930**, *26*, 376; b) J. C. Slater, *Phys. Rev.* **1951**, *81*, 385; c) S. H. Vosko, L. Wilk, M. Nussiar, *Can. J. Phys.* **1980**, *58*, 1200; d) A. D. Becke, *Phys. Rev.* **1988**, *A38*, 3098; e) J. P. Perdew, *Phys. Rev.* **1986**, *B33*, 8822; J. P. Perdew, *Phys. Rev.* **1986**, *B34*, 7406.

[25] a) F. Bernardi, A. Bottoni, M. Calcinari, I. Rossi, M. A. Robb, *J. Phys. Chem.* **1997**, *101*, 6310; b) V. R. Jensen, K. Børve, *J. Comput. Chem.* **1998**, *19*, 947.

[26] a) A. H. J. Wachters, *J. Chem. Phys.* **1970**, *52*, 1033; b) P. J. Hay, *J. Chem. Phys.* **1977**, *66*, 4377; c) N. Godbout, D. R. Salahub, J. Andzelm, E. Wimmer, *Can. J. Chem.* **1992**, *70*, 560; d) TURBOMOLE basis set library.

[27] A. E. Reed, L. A. Curtiss, F. Weinhold, *Chem. Rev.* **1988**, *88*, 899.

[28] K. R. Hanson, *J. Am. Chem. Soc.* **1966**, *88*, 2731.

[29] H. Yasuda, A. Nakamura, *Angew. Chem.* **1987**, *99*, 745; *Angew. Chem. Int. Ed. Engl.* **1987**, *16*, 723.

[30] For the η^3-π-butenyl – metal coordination, the supine/prone notation[29] is given in addition to the *Re*/*Si* terminology.[28] The two enantiomers for the $\eta^1(C^1)$- as well as the $\eta^1(C^3)$-butenyl – metal coordination can be envisioned in a similar way. The *Re*/*Si* terminology is applied with regard to the chirality of the C^3 atom in the butenyl group.

[31] In contrast to our previous investigation,[7b] in the present study the real rotational transition-state structures for *anti* – *syn* isomerization are reported.

[32] The catalyst model **I** shows that the equilibrium between π-butenyl (**2π**) and σ-butenyl (**2σ**, **2σ′**) forms of **2** involves a bimolecular step, namely **2π** + ethylene → **2σ** or **2σ′**, which is energetically disfavored because of the decrease in entropy associated with ethylene coordination. In order to ensure an energetically balanced description of elementary steps that involves σ- and π-butenyl species, we are focusing here on ΔH and ΔH^{+}.

[33] SPY species of **2σ** and **2σ′**, where *cis*-butadiene occupies two basal positions, are calculated to be $\approx 7-9$ kcal mol^{-1} (ΔH) thermodynamically less stable relative to TBPY species.

[34] Stereoisomers that differ in the chirality of the butenyl – Ni^{II} coordination (supine/prone or *Re*/*Si*) are found to be very close in energy for $\eta^1(C^1)$ **2σ** and of $\eta^1(C^3)$ **2σ′** forms of **2**, and also for η^1-butenyl **3σ** and η^3-butenyl **3π** insertion transition, for both *anti* and *syn* forms. Average values were therefore used in the determination of thermodynamic stabilities as well as kinetic barriers.

[35] a) J. W. Faller, M. E. Thomsen, M. J. Mattina, *J. Am. Chem. Soc.* **1971**, *93*, 2642; b) J. Lukas, P. W. N. M. van Leeuwen, H. C. Volger, A. P. Kouwenhoven, *J. Organomet. Chem.* **1973**, *47*, 153; c) K. Vrieze in *Dynamic Nuclear Magnetic Resonance Spectroscopy* (Eds.: L. M. Jackman, F. A. Cotton), Academic Press, New York, **1975**.

Received: April 11, 2002 [F4011]

  0947-6539/02/0820-4766 $ 20.00+.50/0